Ceramics International 50 (2024) 12158–12166

Contents lists available at ScienceDirect

Ceramics International

journal homepage: www.elsevier.com/locate/ceramint

Synthesis, sintering, mechanical properties, and oxidation behavior of $(Zr_{0.5}Me_{0.5})B_2$ (Me = Ta, Hf) solid solutions

Simone Barbarossa [a], Mariano Casu [a], Roberto Orrù [a,*], Antonio M. Locci [a], Giacomo Cao [a], Sebastiano Garroni [b], Devis Bellucci [c], Valeria Cannillo [c]

[a] Dipartimento di Ingegneria Meccanica, Chimica, e Dei Materiali, Unità di Ricerca Del Consorzio Interuniversitario Nazionale per La Scienza e Tecnologia Dei Materiali (INSTM), Università Degli Studi di Cagliari, Via Marengo 2, 09123, Cagliari, Italy
[b] Dipartimento di Scienze Chimiche, Fisiche, Matematiche e Naturali, Università Degli Studi di Sassari, 07100, Sassari, Italy
[c] Dipartimento di Ingegneria "Enzo Ferrari", Università di Modena e Reggio Emilia, Via P. Vivarelli 10, 41125, Modena, Italy

ARTICLE INFO

Handling editor: P. Vincenzini

Keywords:
Solid solution
Borides
Self-propagating high-temperature synthesis
Spark plasma sintering
Oxidation resistance

ABSTRACT

In this work, $(Zr_{0.5}Ta_{0.5})$ B_2 and $(Zr_{0.5}Hf_{0.5})$ B_2 solid solutions are produced in dense form by coupling the Self-propagating High-temperature (SHS) and Spark Plasma Sintering (SPS) routes. A single boride phase solid solution is formed in both cases by SPS (1850 °C, 20 min) from the multiphasic ceramic powders preliminarily obtained by SHS. The use of small amounts of graphite during SPS is highly beneficial to eliminate oxide contaminants (from 14.5–16.0 wt% to 2.1–2.8 wt%), improve powder consolidation (from 87-90 % to 97.5–98 %), and make the operating conditions milder. Better mechanical properties are exhibited by the binary ceramics with respect to ZrB_2 produced by SHS-SPS. The presence of Ta makes the performance of $(Zr_{0.5}Ta_{0.5})B_2$ superior compared to the Hf-containing system, with hardness, Young's modulus, and fracture toughness equal to 22.1 GPa, 636.9 GPa, and 2.46 MPa $m^{1/2}$, respectively. On the other hand, $(Zr_{0.5}Hf_{0.5})$ B_2 shows higher oxidation resistance in flowing and stagnant air at elevated temperatures.

1. Introduction

It is well recognized that the unusual combination of desirable chemical and physical properties (including high melting points, good thermal stability, elevated hardness, high thermal conductivity, etc.) make Ultra-High Temperature Ceramics (UHTCs) based on transition metal diborides very attractive for various high-temperature applications [1,2]. Such interest prompted several research groups to propose, develop and optimize different processing routes to produce them in bulk form and to characterize in detail the obtained products [1,2]. These studies were mostly addressed to individual diborides, either additive-free or secondary phases-containing, particularly ZrB_2- [3,4], HfB_2- [3,5], and TaB_2- [4] based ceramics. More recently, the novel class of High Entropy Borides (HEBs), where four to five metal cations are combined in near-equimolar proportions to form thermodynamically stable single-phase crystalline solid solutions, have also gained a significant attention [6]. In contrast, binary and ternary metal diborides have been relatively much less explored. In this context, $(Zr,Me)B_2$ solid solutions (with Me = Hf or Ta) are very promising as materials for extreme environments.

By virtue of the prominent role played by Zr- and Hf-diborides in this field, in addition to the displayed mutual solubility in the whole compositional range, $(Zr_xHf_{1-x})B_2$ represents the most investigated binary system [7–10]. A nearly full dense $(Zr_{0.97}Hf_{0.03})B_2$ solid solution was obtained by a multistep HP process (T_{max} equal to 2150 °C) starting from ball milled ZrB_2, and HfB_2 powders [7]. The latter precursors were also co-milled in different proportions for 3 h (CR = 10) by Sitler et al. [8,9] and the resulting mixtures consolidated by Spark Plasma Sintering (5 kN, 1700 °C, 10 min) to obtain bulk $(Zr_{0.2}Hf_{0.8})B_2$ (relative density, ρ = 76.5 %), $(Zr_{0.5}Hf_{0.5})B_2$ (ρ = 76.2 %), and $(Zr_{0.8}Hf_{0.2})B_2$ (ρ = 82.9 %) solid solutions. More recently, flash sintering of $(Hf_{0.5}Zr_{0.5})B_2$ was accomplished by Belisario et al. [10] starting from powders synthesized either from carbothermal reduction (CTR) or borohydride reduction (BHR). The latter method was considered preferable in terms of product densification (about 70 and 95 % dense, for CTR and BHR, respectively), hardness (8.23 ± 0.10 and 23.01 ± 0.37 GPa, respectively), and oxidation resistance.

The synthesis of $(Zr_{1-x}Ta_x)B_2$ solid solutions (x from 0 to 1) was first

* Corresponding author.
E-mail address: roberto.orru@unica.it (R. Orrù).

https://doi.org/10.1016/j.ceramint.2024.01.119
Received 30 October 2023; Received in revised form 22 December 2023; Accepted 8 January 2024
Available online 9 January 2024

attempted by arc melting starting from ZrB_2, and TaB_2 [11]. Based on the XRD analysis, it was concluded that the stable compositional range for this system was Ta ≤8 % mol. Consistently, a single phase $(Zr_{0.97}Ta_{0.03})B_2$ solid solution was obtained by McClane et al. [12] using a multistep program by HP (T_{max} equal to 2150 °C) while starting from ball milled ZrB_2, and Ta powders. Furthermore, Zr-rich $(Zr_{1-x}Ta_x)B_2$ products (x = 0.03 and 0.06) have been also prepared via a multistep reactive HP method (T_{max} = 2200 °C) preceded by a hydride-based synthesis technique from ZrH_2, amorphous B, phenolic resin, and Ta_2H precursors [13]. The resulting products possessed relative densities of 99.2 and 99.0 %, respectively, and consisted of the desired solid solutions with small amounts of ZrC and ZrO_2. The same processing route was also subsequently adopted for the preparation of $(Zr_{0.5}Ta_{0.5})B_2$ [14]. The resulting 95.9 % dense ceramic was not single-phase, while a core–shell microstructure, consisting of ZrB_2 cores surrounded by shells of $(Zr,Ta)B_2$ solid solutions, was formed. More recently, the preparation of $(Zr_{1-x}Ta_x)B_2$ in a wide compositional range (x = 0–0.95) was investigated by Vorotilo et al. [15] by HP (1900°C, 50 MPa, 10 min) of powders obtained by Self-propagating High-temperature Synthesis (SHS) after a 4 h long ball milling treatment (CR = 6) of Zr, Ta, and B precursors. It was found that the highest Ta content allowable to form a single-phase product was 25–27 at.%, whereas, above the latter limit (for instance the $(Zr_{0.5}Ta_{0.5})B_2$ system), a multiphasic product was obtained. Therefore, based on the information provided above and to the best of our knowledge, the equiatomic $(Zr,Ta)B_2$ solid solution was not obtained so far in the literature as single boride phase.

In the present work, the fabrication of nearly full dense and single boride phase $(Zr_{0.5}Hf_{0.5})B_2$ and $(Zr_{0.5}Ta_{0.5})B_2$ solid solutions is attempted using the SHS-SPS route, consisting in the processing by SPS of the powders preliminarily synthesized by SHS. The latter two-step approach was demonstrated to be very effective for the obtainment not only of standard MeB_2 (Me = Zr, Hf, Ta, and Ti) in bulk form [4,5,16] but also for the production of different dense quinary HEBs [17–20]. In the latter regard, following the beneficial influence deriving from the introduction of small amounts of graphite to the SHS powders prior to SPS, to remove O-contaminants and concurrently improving HEBs consolidation, the effect of this additive will be also examined for the case of the two binary diboride systems above. The optimal sintered products will be finally characterized from the mechanical and oxidation points of view and the obtained results will be compared.

2. Experimental materials and methods

2.1. Self-propagating high-temperature synthesis and Spark Plasma Sintering

Zirconium (Alfa Aesar, cod 00847, APS 2–3 μm), hafnium (Alfa Aesar, cod. 10,201, 99.6 % pure, <44 μm), tantalum (Alfa Aesar, cod 00337, particle size <44 μm, 99.9 % pure), and amorphous boron (Sigma-Aldrich, cod 15,580, ≥99 % pure) powders were used for the synthesis by SHS of $(Zr_{0.5}Ta_{0.5})B_2$ and $(Zr_{0.5}Hf_{0.5})B_2$, according to the following reaction stoichiometry:

$$0.5Zr + 0.5Me + 2B \rightarrow (Zr_{0.5}Me_{0.5})B_2,\ Me = Ta, Hf \quad (1)$$

A 10 mol.% excess of boron was used to compensate its additional consumption for the borothermal reduction of oxides present on the powder precursors surface. The two batches were first mixed under very mild conditions (20 min, ball to powder weight ratio equal to about 0.2, plastic vials and alumina balls) in a SPEX 8000 (SPEX CertiPrep, USA) shaker mill and then uniaxially cold-pressed with no binder to form cylindrical pellets to be reacted by SHS. Once locally ignited by an electrically heated tungsten filament (R.D. Mathis, USA), the synthesis process occurred in few seconds inside a stainless-steel chamber, under Argon environment.

After SHS, the obtained porous products were processed, without or in presence of 1 wt% graphite (Sigma-Aldrich, cod 282,863, <20 μm), for 1 h by ball milling (SPEX CertiPrep, USA, ball to powder weight ratio of 2, hardened steel milling media).

Particle size distribution of the SHS powders was evaluated by laser light scattering analysis (CILAS 1180, France).

Additive free and graphite containing mixtures were consolidated by SPS (515S model apparatus, Fuji Electronic Industrial Co., Ltd., Kanagawa, Japan) under vacuum conditions (about 20 Pa). The process was conducted under temperature-controlled mode using an infrared pyrometer (CHINO, mod. IR-AHS2, Japan) focused on the lateral surface of a cylindrical graphite die (30 mm external diameter; 15 mm inside diameter; 30 mm height). The dwell temperature (T_D), heating rate, holding time, and applied pressure values during SPS runs were 1850 °C (1 wt%C) or 1950 °C (0 wt%C), about 200 °C/min, 20 min, and 20 MPa, respectively. The resulting sintered samples were cylindrical disks of about 15 mm diameter and 3 mm height. Further details on SHS and SPS experiments can be found in previous works [18,19,21].

2.2. Products composition and microstructure

Phases identification in SHS and SPS products was carried out by X-ray diffraction using a SMARTLAB diffractometer with a rotating anode source of copper (λCu Kα = 1.54178 Å) working at 40 kV and 100 mA over a range of scattering angles 2ϑ from 20° to 80°, in steps of 0.05° with 15 s acquisition time per angle step. The diffractometer is equipped with a graphite monochromator and a scintillation tube in the diffracted beam. The Rietveld method was used to estimate phases amount (wt.%) and the corresponding structural parameters by analyzing the XRD patterns with the MAUD program [22].

The Archimedes' method, using distilled water as immersion medium, was employed to determine the absolute density of SPS samples. The corresponding relative densities were calculated by considering the crystallographic values (ρ_c) of 9.10 and 8.59 g/cm^3 for $(Zr_{0.5}Ta_{0.5})B_2$ and $(Zr_{0.5}Hf_{0.5})B_2$, respectively, estimated according to the Rietveld's analysis results by using the following formula:

$$\rho_c = (Z \cdot M/V_c) \cdot (10^{24}/N_A)$$

where Z is the stoichiometry of each element, M the corresponding molar mass, V_c the volume of the lattice cell, and N_A the Avogadro constant. The presence of graphite (2.26 g/cm^3) in 1 wt%C samples was also accounted for the evaluation of their theoretical densities, as described elsewhere [18].

SHSed powders and sintered samples microstructures were examined by high resolution scanning electron microscopy (HRSEM) (mod. S4000, Hitachi, Tokyo, Japan) equipped with an UltraDry EDS Detector (Thermo Fisher Scientific, Waltham, MA, USA).

2.3. Oxidation resistance and mechanical properties

Thermogravimetric analysis tests (NETZSCH, STA 409 PC Luxx Simultaneous DTA-TGA Instrument, Germany) were conducted under 0.1 L/min air flow to evaluate the oxidation behavior of the two binary metal diborides. Specifically, the optimal products of both systems were subjected to non-isothermal (dynamic) experiments, consisting of slowly heating (2 °C/min) small parallelepiped sized pieces, from room temperature to 1450 °C. The resulting normalized weight changes, expressed as $\frac{mg}{cm^2}$, are compared with those relative to dense ZrB_2 [4], TaB_2 [4], and HfB_2 [23] ceramics produced by SHS-SPS or reactive SPS. Additional oxidation experiments on sintered samples were carried out in a muffle furnace in stagnant air (LT 24/11/B410, Nabertherm, Lilienthal, Germany). During these tests, samples were heated at a rate of 4 °C/min from room temperature to a maximum value, in the range of 600–1200 °C, followed by an isothermal step of 1 h duration. The surface changes of heat-treated specimens were then examined by XRD and SEM.

2.4. Mechanical properties

The Young's modulus and hardness of the different samples were assessed using the micro-indentation technique. The evaluations were conducted utilizing the Open Platform equipment (CSM Instruments, Peseux, Switzerland), employing a Vickers indenter tip. The indentation process applied a 1 N load with a loading/unloading rate of 2 N/min, and the maximum load was sustained for 15 s. A minimum of 15 measurements were taken for each sample, and an automatic recording of the load-penetration depth curve was made for each indentation. Subsequently, the elastic modulus was determined using the Oliver and Pharr method, which relies on the indentation load-unloading curves [24]. Additionally, fracture toughness was evaluated using a load of 3 N in order to make cracks propagate from the indent tips. Fracture toughness was then calculated based on the crack lengths according to widely used equations available in the literature [25,26].

3. Results and discussion

3.1. Processing and microstructural characterization

3.1.1. The $(Zr_{0.5}Ta_{0.5})B_2$ system

As for the corresponding ZrB_2 and TaB_2 constituents [4], the synthesis reaction for the formation of $(Zr_{0.5}Ta_{0.5})B_2$ according to Eq. (1) displayed an SHS behavior. However, in the present study, reactants were not fully converted into the desired binary phase, as shown in Fig. 1 and Supplementary Table S1, with the resulting product consisting of ZrB_2 and TaB_2, and a mixture of binary solid solutions with different Zr/Ta stoichiometric molar ratio. The latter values were nominally estimated by applying the Vegards' law. More specifically, a good agreement between experimental and calculated fit was obtained by considering $(Zr_{0.26}Ta_{0.74})B_2$, $(Zr_{0.35}Ta_{0.65})B_2$, and $(Zr_{0.08}Ta_{0.92})B_2$, other than the individual diborides. Additional secondary phases, in particular metal oxides, are also most likely present, even though they were not clearly detectable by this analysis, due to the corresponding XRD pattern complexity.

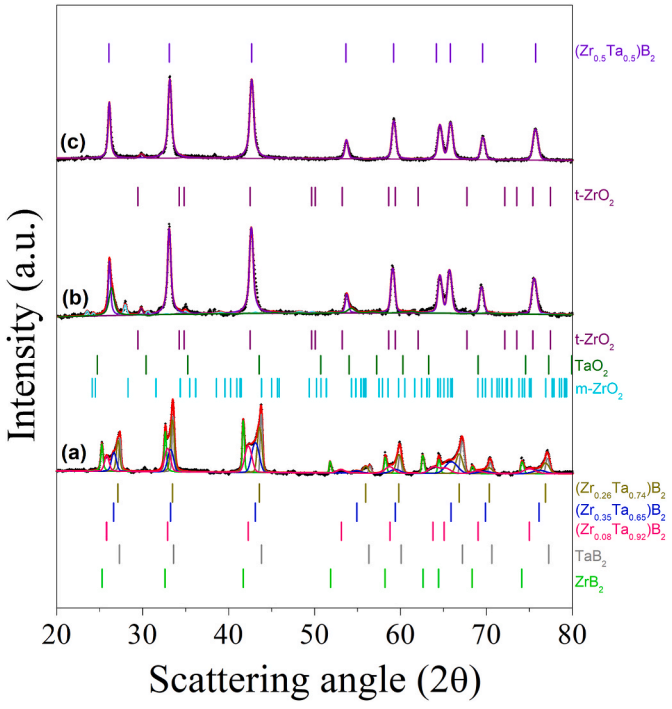

Fig. 1. XRD patterns of $(Zr_{0.5}Ta_{0.5})B_2$ products: SHS powders (a), and SPS bulk samples obtained with no additive at $T_D = 1950$ °C (b) and in presence of 1 wt% graphite at $T_D = 1850$ °C (c). Red dots are experimental data, the continuous lines are the calculated best fit. (For interpretation of the references to colour in this figure legend, the reader is referred to the Web version of this article.)

SHS powders were also examined by SEM and EDS, and the obtained results are shown in Supplementary Fig. S1a. The SEM micrograph evidences that powders consist of aggregates of very fine grains. Moreover, in accordance with the XRD analysis results described above, elemental maps proved that Tantalum and Zirconium are not uniformly distributed in the SHS product, as confirmed by the small spots present in the elemental maps showing higher concentration of one of the two metallic constituents. Despite this, the latter ones are quite well mixed across each grain, which is expected to favour the formation of the prescribed binary diboride phase during the subsequent SPS stage. EDS analysis also evidenced the presence of oxides on the particles surface.

Apparently, the SHS process takes place too fast to allow Zr and Ta elements to properly diffuse across the sample volume and, finally, form the prescribed equiatomic solid solution. To this aim, as observed for the case of quinary metal diborides [18,19,21], prolonged heat treatments at high temperatures are needed.

Prior to their consolidation, the SHS powders were subjected to a ball milling treatment for 1 h and the resulting particle size parameters were $d_{10} = 0.30 \pm 0.08$ μm, $d_{50} = 1.18 \pm 0.08$ μm, $d_{90} = 9.26 \pm 2.72$ μm, and $d_{43} = 3.09 \pm 0.46$ μm.

As reported in Fig. 1 and Supplementary Table S1, all secondary diboride phases were transformed to $(Zr_{0.5}Ta_{0.5})B_2$ when the additive free powders were processed for 20 min at 1950 °C by SPS. As a drawback, the sintered samples were rich of oxide contaminants, namely ZrO_2 (tetragonal and monoclinic) and TaO_2 (tetragonal). The latter ones are also responsible for the scarce powder densification level, only 87 %, achieved during SPS. Thus, following the positive effects deriving from the addition of small amounts (1 wt%) of graphite to the SHS powders before the sintering step, as observed for the case of HEBs [18,19], the same procedure was adopted also in the present investigation. Correspondingly, 99 % dense products were obtained when operating at $T_D = 1950$ °C. Furthermore, since the presence of graphite was found beneficial not only for reducing undesired oxides and improving samples consolidation, but also to enhance powders reactivity thus making the required SPS conditions milder [20], the dwell temperature was lowered to 1850 °C. A 97.5 % dense sample consisting of $(Zr_{0.5}Ta_{0.5})B_2$ with only small amounts of ZrO_2, about 2.5 wt% (cf. Fig. 1 and Supplementary Table S1), was correspondingly produced.

The results above are confirmed by the SEM micrographs and the related elemental EDS maps shown in Fig. 2a–b, where the samples sintered at 1950 °C (0 wt%C) and at 1850 °C (1 wt%C) are compared. Despite the obtained uniform elements' distribution, the ceramic sintered at $T_D = 1950$ °C with no graphite is characterized by a marked residual porosity and the presence of a significant amount of metal oxides, mostly confined inside the pores, as seen in Fig. 2a. On the other hand, Fig. 2b shows that the specimen produced at $T_D = 1850$ °C with 1.0 wt%C is nearly full densified with Zr and Ta homogeneously distributed across the sample volume, with a marked reduction of O-contaminants. The latter statement is also supported by EDS patterns reported in Supplementary Fig. S2.

It should be emphasized that, based on the state of the art, the $(Zr_{0.5}Ta_{0.5})B_2$ solid solution is obtained for the first time in the present work as a single boride phase. The latter goal was not achieved in the literature even when considering this ceramic system in powder form. For instance, the molten salt synthesis route was used by Wen et al. [27] to prepare various binary metal diborides, including $(Zr_{0.5}Ta_{0.5})B_2$. In the latter case, the resulting product was characterized by multiple phases of metal diborides. Furthermore, their experimental findings agreed with a theoretical criterion based on combinatorial methods the same authors developed to predict the formation of binary metal diboride solid solutions. The fact that the results obtained in our work are in contradiction with such prediction means that the adopted criterion unequivocally presents some limitations. Therefore, more detailed theoretical studies are required to establish a priori the

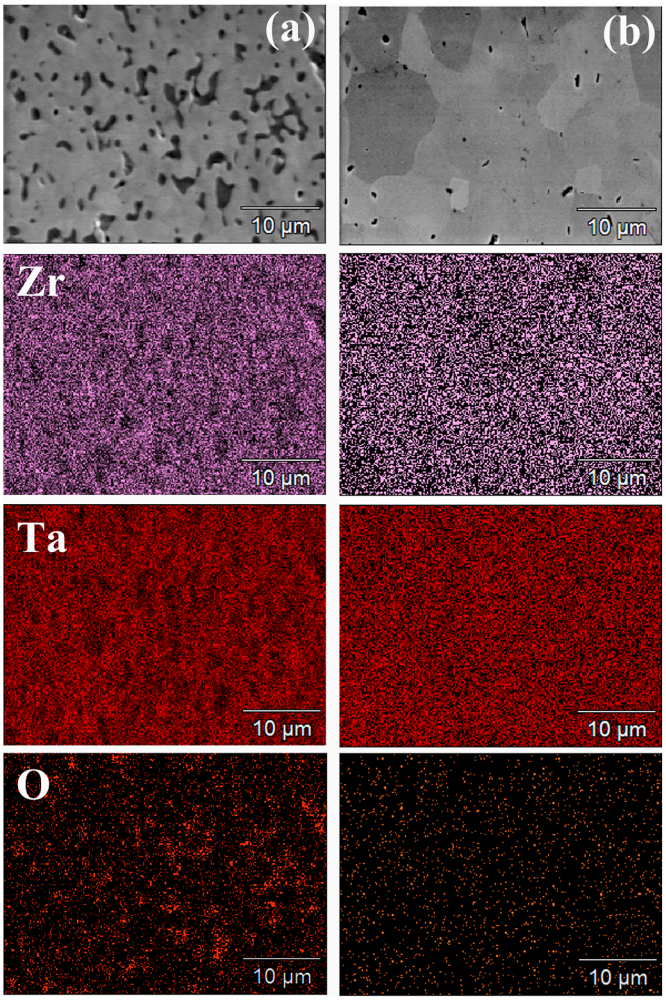

Fig. 2. Cross sectional SEM micrographs and related EDS elemental maps of $(Zr_{0.5}Ta_{0.5})B_2$ samples obtained by SPS at (a) T_D = 1950 °C with no graphite, and at (b) T_D = 1850 °C in presence of 1 wt% graphite.

formation of this type of binary solutions.

3.1.2. *The $(Zr_{0.5}Hf_{0.5})B_2$ system*

As for the previous system, also the synthesis of $(Zr_{0.5}Hf_{0.5})B_2$ from elemental powders showed an SHS character upon local ignition. The XRD pattern of the resulting powders is reported in Fig. 3, whereas the related phases' amount and microstructural parameters estimated by the Rietveld method are listed in Supplementary Table S2. A multiphasic ceramic is also obtained in this case: other than the expected $(Zr_{0.5}Hf_{0.5})B_2$ solid solution (21.3 wt%), the additional detected phases by XRD were HfB_2 (31.2 wt%), ZrB_2 (43.0 wt%), and unreacted Zr (4.5 wt%).

SEM/EDS observations of SHS powders agree with XRD outcomes. As for the case of $(Zr_{0.5}Hf_{0.5})B_2$, elemental maps reported in Supplementary Fig. S1b evidenced a good but not homogeneous distribution of the two metallic constituents in the synthesized powders. Furthermore, O-contaminants are also detected on particles surface.

After being ball milled for 1 h ($d_{10} = 0.18 \pm 0.03$ μm, $d_{50} = 1.1 \pm 0.1$ μm, $d_{90} = 7.3 \pm 0.3$ μm, and $d_{43} = 2.6 \pm 0.1$ μm), the SHS powders were then sintered either with no graphite or after being combined with 1 wt % of this additive. In the first case, the consolidation by SPS at 1950 °C led to a 90 % dense sample consisting of the desired binary phase, with neither additional diborides nor residual reactants, but with a significant content on metal oxides (ZrO_2 and HfO_2), estimated to be about 14.5 wt % in total (cf. Fig. 3 and Supplementary Table S2). As evidenced by the corresponding SEM micrograph shown in Fig. 4a along with the related

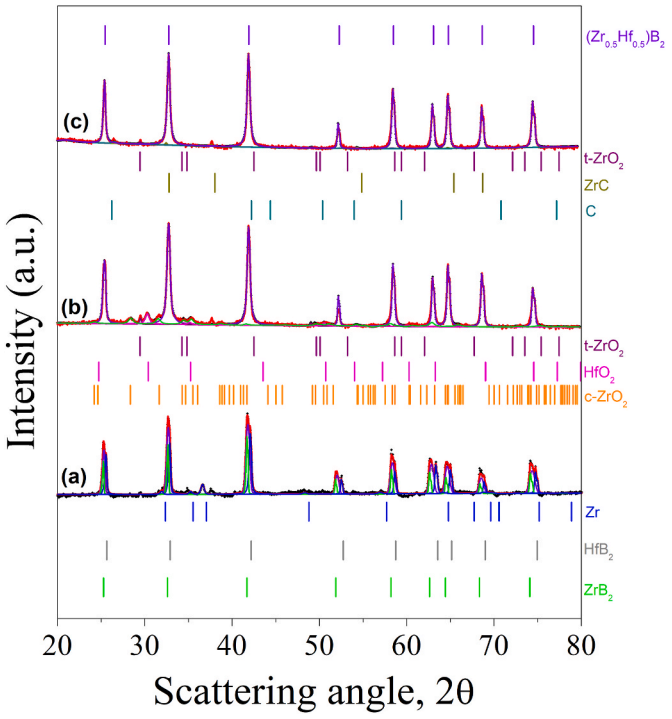

Fig. 3. XRD patterns of $(Zr_{0.5}Hf_{0.5})B_2$ products: SHS powders (a), and SPS bulk samples obtained with no additive at T_D = 1950 °C (b) and in presence of 1 wt% graphite at T_D = 1850 °C (c). Red dots are experimental data, the continuous lines are the calculated best fit. (For interpretation of the references to colour in this figure legend, the reader is referred to the Web version of this article.)

elemental maps, various large pores, up to 4–5 μm sized, are present in this samples. A marked removal of oxide impurities (down to 2.1 wt%) is produced, along with the simultaneous increase of sample densification (up to 98 %), when SHS powders were processed at 1850 °C by SPS with 1 wt% graphite. Traces of ZrC (0.6 wt%) and residual graphite (0.7 wt%) were also detected in the sintered product. The decreased residual porosity is confirmed by the related cross-sectional SEM image reported in Fig. 4b. In addition, pores size is significantly reduced, compared to the sample produced at 1950 °C with no graphite, to about 1 μm. A very homogeneous Zr and Hf distribution is also achieved, as demonstrated by the elemental maps shown Fig. 4b. The significant reduction of oxides content in the sintered products is also confirmed by EDS analysis (see also Supplementary Fig. S3).

While the $(Zr_{0.5}Ta_{0.5})B_2$ system was obtained as a single boride phase for the first time in the present investigation, other authors already succeeded, as mentioned in the Introduction, in the fabrication of bulk $(Zr_{0.5}Hf_{0.5})B_2$, with no additional secondary diborides [7–10]. Nonetheless, except for the investigation conducted by Belisario et al. [10], who make use of Flash Sintering to obtain about 95 % dense ceramics, more severe temperature levels, compared to the optimal (1850 °C) considered in the present study, were required to achieve adequate consolidation levels. In particular, a maximum temperature of 2150 °C was needed to McClane et al. [7] for the obtainment of 99.5 % dense $(Zr_{0.5}Hf_{0.5})B_2$. On the other hand, the very mild conditions (1700 °C) tested by Sitler et al. [8,9] corresponded to scarcely densified samples (76.2 %). The recognized high sintering ability of SHS powders [28,29], the utilization of the efficient SPS technology for processing highly refractory ceramics [30], and the beneficial use of graphite as carbothermal reductant and solid lubricant agent [18], are the main factors responsible for such outcome.

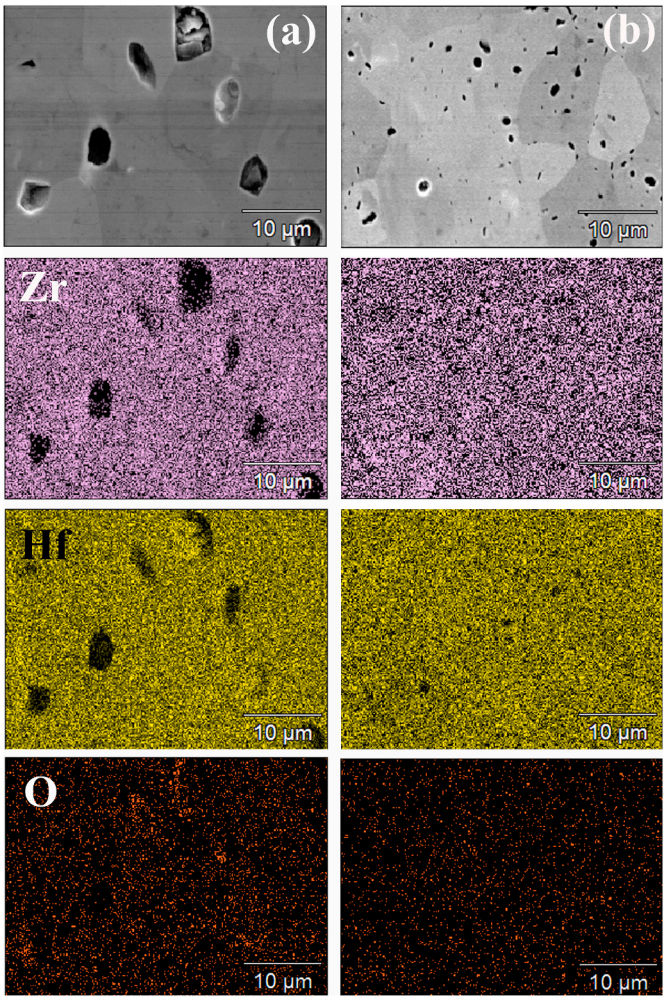

Fig. 4. Cross sectional SEM micrographs and corresponding EDS elemental maps of $(Zr_{0.5}Hf_{0.5})B_2$ samples obtained by SPS at (a) T_D = 1950 °C with no graphite, and at (b) T_D = 1850 °C in presence of 1 wt% graphite.

3.2. Oxidation behavior

The oxidation resistance of the two binary diborides can be preliminarily deduced from the results obtained by dynamic TGA experiments conducted in air flow up to 1450 °C. Fig. 5a–b shows the normalized weight gain as a function of the temperature recorded for the $(Zr_{0.5}Ta_{0.5})B_2$ and $(Zr_{0.5}Hf_{0.5})B_2$ systems, respectively. Literature data relative to the corresponding individual diborides prepared either by the SHS-SPS (ZrB_2, and TaB_2) [4], or reactive SPS (HfB_2) [23] routes are also reported, for comparison. These graphs indicate that, up to 1200–1300 °C, the oxidation curves of both binary diborides are very close to those of the related diboride constituents. As for $(Zr_{0.5}Ta_{0.5})B_2$, ZrB_2, and TaB_2 systems (Fig. 5a), mass changes lower than $\pm 1 \frac{mg}{cm^2}$ were measured up to about 700 °C, above which the three diborides start to gain weight at rates in the range of $4.8–6.0 \cdot 10^{-3} \frac{mg}{cm^2 °C}$ which remained about constant until a temperature of approximately 1200 °C was reached. As the test proceeded, these ceramics oxidized at higher rates, with the TGA curves of $(Zr_{0.5}Ta_{0.5})B_2$, and ZrB_2 almost overlapped. On the other hand, TaB_2 was much more sensitive to the oxidizing environment, as proven by the corresponding sudden raise of the related curve (Fig. 5a). This fact is responsible for the superior oxidation resistance of the $(Zr_{0.5}Ta_{0.5})B_2$ system with respect to the average performances of ZrB_2 and TaB_2, as evidenced in Supplementary Fig. S4a. However, it should be pointed out that the lower relative density (higher porosity) of the latter sample (93.9 %), compared to those of ZrB_2 (98.5 %) and $(Zr_{0.5}Ta_{0.5})B_2$ (97.5 %), is expected to negatively affect its oxidation behavior.

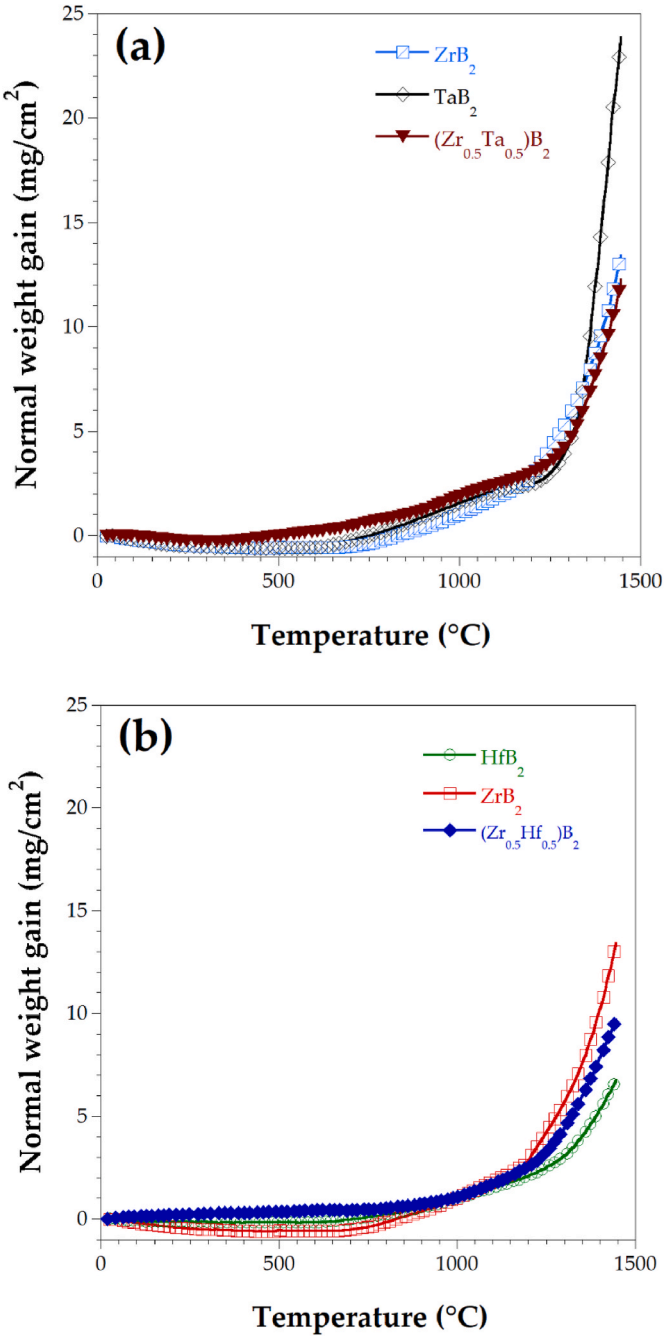

Fig. 5. Specific weight changes during TGA oxidation test in air of (a) $(Zr_{0.5}Ta_{0.5})B_2$ and (b) $(Zr_{0.5}Hf_{0.5})B_2$ samples produced in this work by SPS (T_D = 1850 °C, 1 wt%C) as a function of temperature (heating rate equal to 2 °C/min). Literature data of individual diborides, i.e. HfB_2 (ρ = 98.8 %) [23], ZrB_2 (ρ = 98.5 %) [4], and TaB_2 (ρ = 93.9 %) [4] are also reported for comparison.

Fig. 5b shows that the normalized weight changes of $(Zr_{0.5}Hf_{0.5})B_2$, ZrB_2, and HfB_2 samples is quite modest, i.e. within $\pm 1 \frac{mg}{cm^2}$, up to about 1000 °C. As temperature exceeded the latter level, an increased mass gain rate was recorded during the test, with the oxidation curve of the binary system in between to those ones corresponding to the individual constituents. The oxidative behavior displayed by the $(Zr_{0.5}Hf_{0.5})B_2$ sample produced in this work is in line with the results of TGA-DSC tests in flowing air conducted on the bulk sample (95 % relative density) fabricated by Flash Sintering (FS) from powders synthesized by borohydride reduction (BHR) [10]. Indeed, the weight gain recorded at

1440 °C in the latter study (about 2.8 wt%) was only slightly lower than that measured in the present investigation (approximately 3.5 wt% at 1450 °C). As a main difference, a weight loss of about 0.5 % was observed in the temperature range 800–1000 °C in Belisario et al. [10], ascribed by the authors to the evaporation of some amorphous phases formed during the BHR-FS processing steps. Moreover, a significantly lower thermal oxidation resistance (about 9 wt% gain at 1440 °C) was exhibited by the 70 % dense product also obtained by Belisario et al. [10] when starting from powders produced by carbothermal reduction.

Interestingly, as shown in Supplementary Fig. S4b, the weight gain of $(Zr_{0.5}Hf_{0.5})B_2$ is nearly coincident to the average value of the two individual metal diborides. By comparing the three competitors, HfB_2 was found to display the lowest mass change (highest thermal stability) in the entire temperature range. This outcome agrees with literature findings [31], where HfB_2 is typically found to be the most stable transition metal diboride. In addition, this is also consistent with the superior oxidation resistance displayed by $(Zr_{0.5}Hf_{0.5})B_2$ compared to $(Zr_{0.5}Ta_{0.5})B_2$, whose normalized weight gain values achieved at 1450 °C equal to approximately 9.5 (Fig. 5a) and 12 $\frac{mg}{cm^2}$ (Fig. 5b), respectively. Such hierarchical order can be considered representative of the oxidative behavior of the two binary systems, as the relative densities of the two samples subjected to TGA tests were nearly the same, i.e. about 98 and 97.5 %, respectively.

Additional oxidation tests, based on the heat treatment in a furnace of the two systems investigated in this work, have been also carried out. During these experiments, samples were exposed to stagnant air for 1 h at different temperature conditions, in the range 600–1200 °C. As shown in Supplementary Fig. S5, the resulting weight gains are consistent with TGA outcomes (Fig. 5) and confirm that $(Zr_{0.5}Hf_{0.5})B_2$ is more stable under oxidative environments with respect to the Ta-containing ceramic counterpart. This statement is also supported by XRD analysis results reported in Fig. 6a and b. First, the latter ones provide the evidence that the incipient oxides formation occurred at 600 °C. However, although oxidation phenomena proceeded in both systems with the increasing temperature, major effects are produced on $(Zr_{0.5}Ta_{0.5})B_2$ samples, particularly at 800 °C (Fig. 6a). Indeed, XRD peaks of the diboride phase can be barely detected in the corresponding pattern of the latter system. Conversely, the analysis relative to the other binary product indicates that the original boride phase is still significantly present at 800 °C (Fig. 6b). Finally, only metal oxides were detected on the surface of materials heat treated at 1000 and 1200 °C.

The annealed samples were also examined by SEM-EDS. These observations confirmed that an oxide layer, with a progressively growing thickness as the temperature was raised from 600 to 1200 °C, was formed on the sample surface. As an example, the cross-sectional SEM micrographs of $(Zr_{0.5}Ta_{0.5})B_2$, and $(Zr_{0.5}Hf_{0.5})B_2$ specimens processed at 1200 °C are shown in Figs. 7 and 8, respectively, along with the corresponding elemental maps and EDS patterns. The oxide layers formed in both cases under such conditions are characterized by a thickness in the range 40–50 μm. It is also important to note that no changes in the distribution of metallic species is observed upon the annealing process.

The observed higher oxidation resistance of $(Zr_{0.5}Hf_{0.5})B_2$ compared to $(Zr_{0.5}Ta_{0.5})B_2$ depends on kinetic and thermodynamic features. Indeed, a high transport rate through the formed oxide layer would enhance the oxidation of the underlying boride phases. On the contrary, a continuous (i.e., pore-free) layer and a low oxygen diffusivity would provide a passive oxidation protection. Moreover, the thermodynamic stability of the oxide phases also contributes to determine the different oxidation behavior shown by the materials synthesized in this work. However, a clear identification of each contribution which plays a role in this context cannot be provided, at least at this stage, due to the lack of reliable data on oxygen diffusion through tantalum and hafnium oxides. Moreover, the oxidation reaction mechanism needs to be clearly identified in order to draw reliable conclusions. All these aspects will be investigated in more detail in a dedicated future work.

3.3. Mechanical properties

Vickers hardness, Young's modulus, and fracture toughness properties measured on the $(Zr_{0.5}Ta_{0.5})B_2$ and $(Zr_{0.5}Hf_{0.5})B_2$ samples obtained under different processing conditions are reported in Table 1, along with

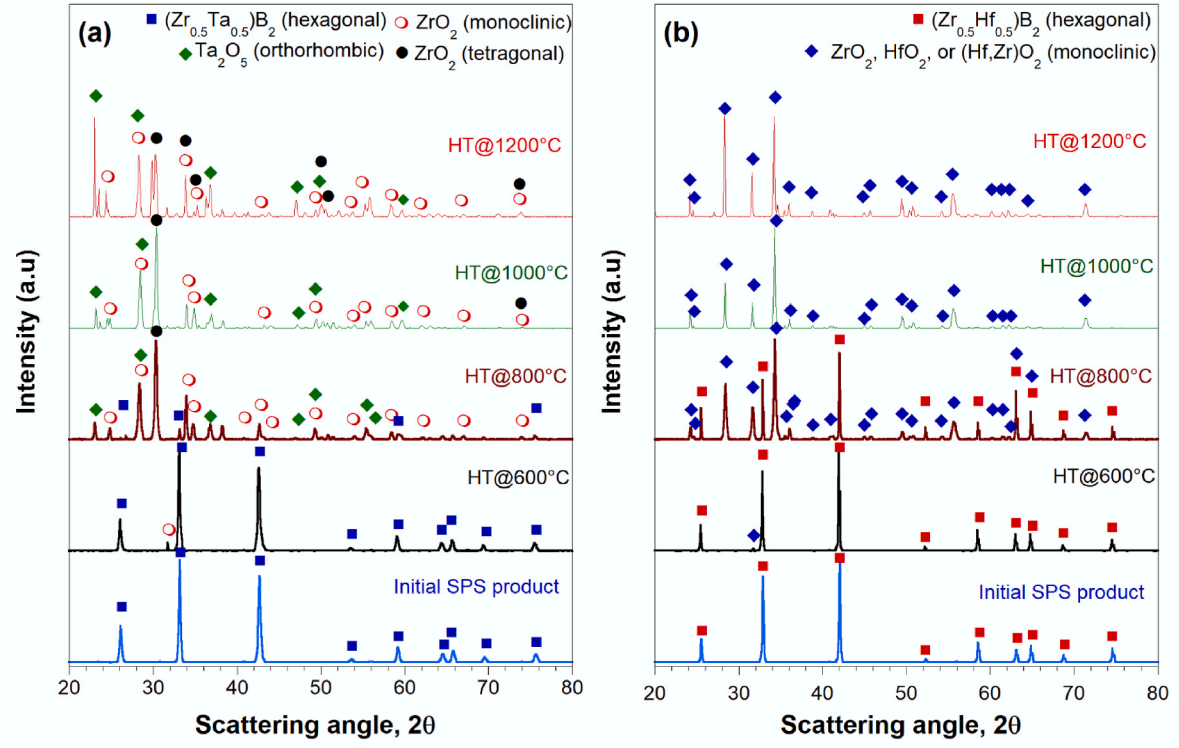

Fig. 6. XRD patterns of (a) $(Zr_{0.5}Ta_{0.5})B_2$, and (b) $(Zr_{0.5}Hf_{0.5})B_2$ samples surface after being heat treated in air furnace at different temperatures.

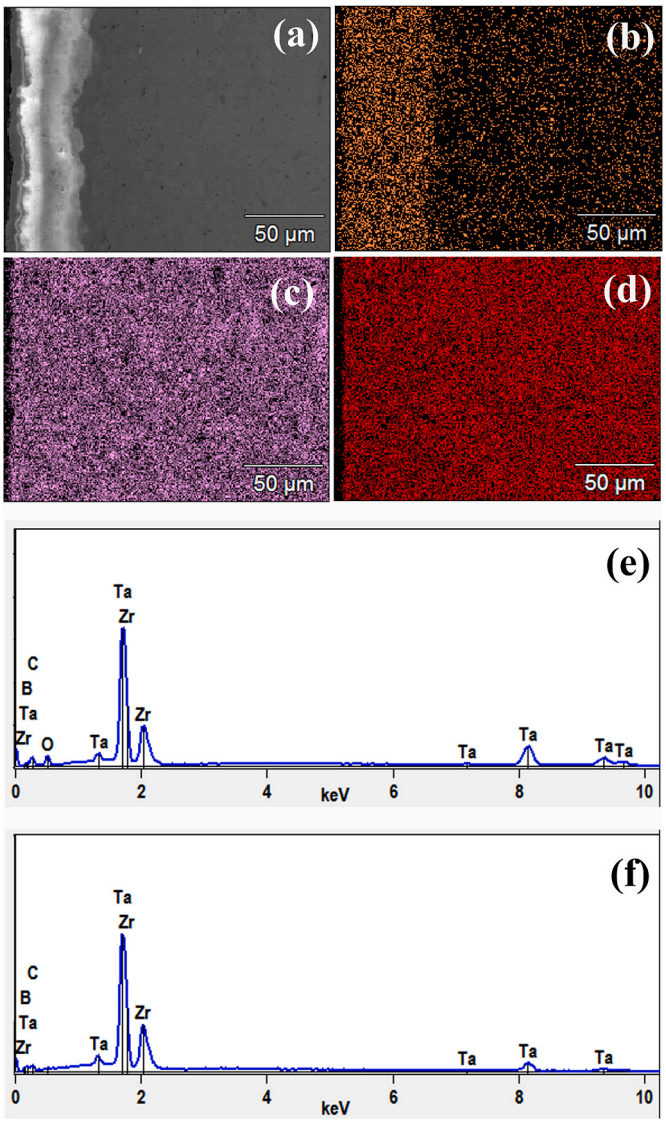

Fig. 7. $(Zr_{0.5}Ta_{0.5})B_2$ sample after heat treatment in air furnace at 1200 °C: (a) cross sectional SEM micrograph, (b) O, (c) Zr, (d) Hf elemental maps, EDS analysis results carried out on (e) the oxide layer, and (f) the bulk material.

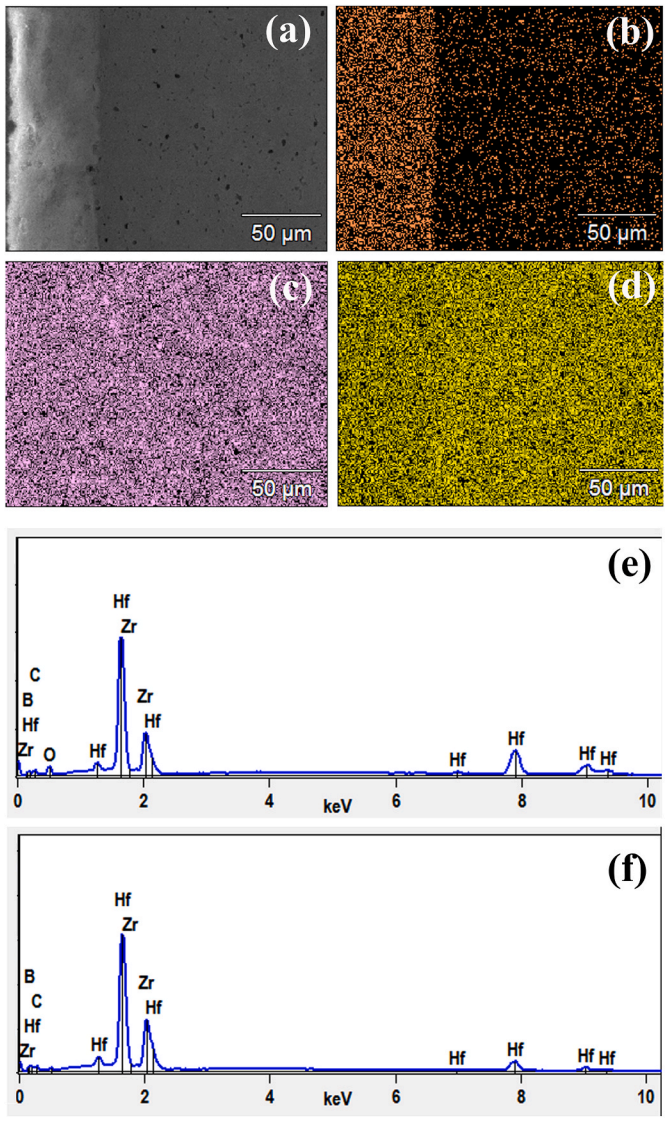

Fig. 8. $(Zr_{0.5}Hf_{0.5})B_2$ sample after heat treatment in air furnace at 1200 °C: (a) cross sectional SEM micrograph, (b) O, (c) Zr, (d) Hf elemental maps, EDS analysis results carried out on (e) the oxide layer, and (f) the bulk material.

the corresponding density values.

It is seen that, the improved densification level (from 87 to 97.5 %) produced, at lower temperature (1850 instead of 1950 °C), with the addition of 1 wt% of graphite to $(Zr_{0.5}Ta_{0.5})B_2$ powders, is also accompanied by a marked increase of both hardness (from 11.37 to 22.08 GPa) and, above all, Young's modulus (from 222.2 ± 9.3 to 636.9 ± 32.9 GPa) in the SPS ceramics. Furthermore, Table 1 indicates that a modest effect was observed when considering K_{IC} values. The mechanical properties obtained for $(Zr_{0.5}Ta_{0.5})B_2$ are quite consistent with those reported in literature for its individual constituents also produced by SHS-SPS [4]. In particular, the combination of ZrB_2 (11.0 ± 0.4 GPa) with the harder TaB_2 made the hardness of the corresponding binary metal diboride product (22.08 ± 0.77 GPa) superior. The fact that the TaB_2 sample displayed a lower HV value (17.5 ± 0.4 GPa) compared to that of $(Zr_{0.5}Ta_{0.5})B_2$ can be readily ascribed to the related modest densification level (93.9 %) [4]. Moreover, the fracture toughness of the binary system (2.46 MPa $m^{1/2}$) was in between to those of ZrB_2 (2.1 MPa $m^{1/2}$) and TaB_2 (3.2 MPa $m^{1/2}$) samples [4].

Similar outcomes were also found when considering the $(Zr_{0.5}Hf_{0.5})B_2$ system, even though less improvements of the mechanical properties are obtained in this case, compared to the Ta-containing diboride. Nonetheless, an increase of both HV and Young's modulus from 15.56 ± 0.49 to 18.40 ± 0.60 GPa and from 428.9 ± 32.1 to 528.2 ± 35.6 GPa, respectively, is achieved with the introduction of graphite and the concurrent decrease of the SPS temperature from 1950 to 1850 °C. The measured HV value of the ceramic produced at 1850 °C/1 wt%C is superior to that of ZrB_2 sample (11.0 ± 0.4 GPa) obtained by SHS-SPS at 1900 °C [4], while it is very close to that of monophasic HfB_2 (18.1 ± 0.4 GPa) prepared by reactive SPS [23]. As for fracture toughness, it should be noted that it was not possible to measure the value for the sample sintered at 1950 °C/0%C, because such sample cracked without the formation of the four cracks at the indent tips. This can be probably ascribed to the residual porosity and local defectiveness.

Based on the results above, lower mechanical properties are displayed by the $(Zr_{0.5}Hf_{0.5})B_2$ system compared to $(Zr_{0.5}Ta_{0.5})B_2$. This finding agrees with the results obtained with HEBs fabricated following the same SHS-SPS processing route [19]. Accordingly, the latter study evidenced that, even if the presence of Ta made the fabrication of fully dense quinary metal borides more difficult, the corresponding ceramics showed superior mechanical properties.

Table 1
Mechanical properties of bulk $(Zr_{0.5}Hf_{0.5})B_2$ and $(Zr_{0.5}Ta_{0.5})B_2$ samples produced by SPS in this work in presence and with no graphite addition. The corresponding processing conditions and density values are also reported. EC: Evans and Charles; LF: Lawn and Fuller; EW: Evans and Wilshaw; L: Lankford. n.d.: not determined.

System	Processing Conditions (T_D, %graphite)	ρ (%)	HV (GPa)	Young's modulus (GPa)	K_{IC} (MPa $m^{1/2}$) Method
$(Zr_{0.5}Ta_{0.5})B_2$	1950 °C, 0%C	87	11.37 ± 0.94	222.2 ± 9.3	2.46 (EC), 1.54 (LF), 6.64 (EW), 1.34 (L)
	1850 °C, 1%C	97.5	22.08 ± 0.77	636.9 ± 32.9	2.46 (EC), 1.53 (LF), 2.33 (EW), 2.28 (L)
$(Zr_{0.5}Hf_{0.5})B_2$	1950 °C, 0%C	90	15.56 ± 0.49	428.9 ± 32.1	n.d. (*)
	1850 °C, 1%C	98	18.40 ± 0.60	528.2 ± 35.6	1.73 (EC), 1.08 (LF), 1.48 (EW), 2.51 (L)

(*)Several cracks formed on the sample during indentation test.

4. Concluding remarks

In this work, equimolar single boride phase (Zr,Ta)B_2 and (Zr,Hf)B_2 solid solutions are produced in bulk form through the SHS-SPS route. The SHS method led in both cases to multiphasic products also containing large amounts of individual borides and other secondary phases. However, when the SHS powders were processed for 20 min by SPS at 1850 °C, with the beneficial presence of 1 wt% graphite, 97.5–98 % dense products basically consisting of the desired $(Zr_{0.5}Ta_{0.5})B_2$ and $(Zr_{0.5}Hf_{0.5})B_2$ phases, with only traces of residual oxides (2.8 and 2.1 wt %, respectively), were obtained.

Both the binary systems displayed superior mechanical properties compared to bulk ZrB_2 produced following the same approach. In particular, $(Zr_{0.5}Ta_{0.5})B_2$ sintered at 1850 °C with 1 wt%C was found to exhibit better mechanical properties, with respect to the Hf-containing system, with hardness, Young's modulus, and fracture toughness equal to 22.1 GPa, 636.9 GPa, and 2.46 MPa $m^{1/2}$, respectively. The opposite outcome is obtained when comparing their oxidation behavior, based on the related results of TGA and furnace experiments in flowing and stagnant air, respectively. Indeed, $(Zr_{0.5}Hf_{0.5})B_2$ displayed better oxidation resistance at high temperature compared to $(Zr_{0.5}Ta_{0.5})B_2$, in agreement with the superior performance, under such conditions, shown by HfB_2 with respect to TaB_2.

In conclusion, in this work it has been demonstrated that the equimolar combination of ZrB_2 with TaB_2 or HfB_2 can provide thermodynamically stable binary diboride solid solutions with improved properties. To this, the consolidation by SPS of powders preliminarily prepared by SHS with the addition of small amounts of graphite represents an efficient route for the fabrication of such multi-element diborides in highly dense form, which have been barely investigated in the literature so far. Work is underway to exploit the same approach for the obtainment of other binary, but also ternary and quaternary, metal diborides with tailored properties.

Declaration of competing interest

The authors declare that they have no known competing financial interests or personal relationships that could have appeared to influence the work reported in this paper.

Acknowledgements

Two of the authors (S.B. and M.C.) performed their activities in the framework of the International Ph.D. in Innovation Sciences and Technologies at the University of Cagliari, Italy. This work was supported by Fondazione di Sardegna (2020) in the framework of the Advanced design of "THErmodinamically-stable Nanocrystalline Alloys (ATHENA)" project, CUP F75F21001370007. This work has been also developed within the framework of the project eINS- Ecosystem of Innovation for Next Generation Sardinia (cod. ECS00000038) funded by the Italian Ministry for Research and Education (MUR) under the National Recovery and Resilience Plan (PNRR) - MISSION 4 COMPONENT 2, "From research to business" INVESTMENT 1.5, "Creation and strengthening of Ecosystems of innovation" and construction of "Territorial R&D Leaders". The authors acknowledge the GAUSS-CeSAR (Centro Servizi d'Ateneo per la Ricerca) of the University of Sassari for X-ray diffraction analyses.

Appendix A. Supplementary data

Supplementary data to this article can be found online at https://doi.org/10.1016/j.ceramint.2024.01.119.

References

[1] W.G. Fahrenholtz, G.E. Hilmas, Ultra-high temperature ceramics: materials for extreme environments, Scripta Mater. 129 (2017) 94–99, https://doi.org/10.1016/j.scriptamat.2016.10.018.
[2] B.R. Golla, A. Mukhopadhyay, B. Basu, S.K. Thimmappa, Review on ultra-high temperature boride ceramics, Prog. Mater. Sci. 111 (2020) 100651, https://doi.org/10.1016/j.pmatsci.2020.100651.
[3] W.G. Fahrenholtz, G.E. Hilmas, I.G. Talmy, J.A. Zaykoski, Refractory diborides of zirconium and hafnium, J. Am. Ceram. Soc. 90 (2007) 1347–1364, https://doi.org/10.1111/j.1551-2916.2007.01583.x.
[4] R. Licheri, C. Musa, R. Orrù, G. Cao, D. Sciti, L. Silvestroni, Bulk monolithic zirconium and tantalum diborides by reactive and non-reactive spark plasma sintering, J. Alloys Compd. 663 (2016) 351–359, https://doi.org/10.1016/j.jallcom.2015.12.096.
[5] C. Musa, R. Licheri, R. Orrù, G. Cao, Synthesis, sintering, and oxidative behavior of HfB_2-$HfSi_2$ ceramics, Ind. Eng. Chem. Res. 53 (22) (2014) 9101–9108, https://doi.org/10.1021/ie4032692.
[6] L. Feng, W.G. Fahrenholtz, D.W. Brenner, High-Entropy ultra-high-temperature borides and Carbides: a New class of materials for extreme environments, Annu. Rev. Mater. Res. 51 (2021) 165–185, https://doi.org/10.1146/annurev-matsci-080819-121217.
[7] D.L. McClane, W.G. Fahrenholtz, G.E. Hilmas, Thermal properties of (Zr,TM)B_2 solid solutions with TM = Hf, Nb, W, Ti, and Y, J. Am. Ceram. Soc. 97 (5) (2014) 1552–1558, https://doi.org/10.1111/jace.13341.
[8] S.J. Sitler, K.S. Raja, I. Charit, ZrB_2-HfB_2 solid solutions as electrode materials for hydrogen reaction in acidic and basic solutions, Mater. Lett. 188 (2017) 239–243, https://doi.org/10.1016/j.matlet.2016.10.122.
[9] S.J. Sitler, K.S. Raja, I. Charit, Hot corrosion behavior of ZrB_2-HfB_2 solid solutions in KCl and K_2SO_4 at 1500°C, Ceram. Int. 43 (18) (2017) 17071–17085, https://doi.org/10.1016/j.ceramint.2017.09.122.
[10] J. Belisario, S. Mondal, I. Khakpour, A. Franco Hernandez, A. Durygin, Z. Cheng, Synthesis and flash sintering of $(Hf_{1-x}Zr_x)B_2$ solid solution powders, J. Eur. Ceram. Soc. 41 (4) (2021) 2215–2225, https://doi.org/10.1016/j.jeurceramsoc.2020.12.015.
[11] S. Otani, T. Aizawa, N. Kieda, Solid solution ranges of zirconium diboride with other refractory diborides: HfB_2, TiB_2, TaB_2, NbB_2, VB_2 and CrB_2, J. Alloys Compd. 475 (1–2) (2009) 273–275, https://doi.org/10.1016/j.jallcom.2008.08.023.
[12] D.L. McClane, W.G. Fahrenholtz, G.E. Hilmas, Thermal properties of (Zr,TM)B_2 solid solutions with TM = Ta, Mo, Re, V, and Cr, J. Am. Ceram. Soc. 98 (2) (2015) 637–644, https://doi.org/10.1111/jace.13341.
[13] A.N. Dorner, K. Werbach, G.E. Hilmas, W.G. Fahrenholtz, Effect of tantalum solid solution additions on the mechanical behavior of ZrB_2, J. Eur. Ceram. Soc. 41 (6) (2021) 3219–3226, https://doi.org/10.1016/j.jeurceramsoc.2020.12.049.
[14] A.N. Dorner, F. Monteverde, W.G. Fahrenholtz, G.E. Hilmas, Solid-state formation mechanisms of core–shell microstructures in (Zr,Ta)B_2 ceramics, J. Am. Ceram. Soc. 105 (5) (2022) 3147–3152, https://doi.org/10.1111/jace.18363.
[15] S. Vorotilo, K. Sidnov, V.V. Kurbatkina, E.A. Levashov, V.V. Klechkovskaya, Superhardening and localized plastic deformation behaviors in ZrB_2 –TaB_2 ceramics, J. Alloys Compd. 901 (2022) 163368, https://doi.org/10.1016/j.jallcom.2021.163368.
[16] E. Sani, M. Meucci, L. Mercatelli, A. Balbo, C. Musa, R. Licheri, R. Orrù, G. Cao, Titanium diboride ceramics for solar thermal absorbers, Sol. Energy Mater. Sol. Cells 169 (2017) 313–319, https://doi.org/10.1016/j.solmat.2017.05.038.
[17] G. Tallarita, R. Licheri, S. Garroni, R. Orrù, G. Cao, Novel processing route for the fabrication of bulk high-entropy metal diborides, Scripta Mater. 158 (2019) 100–104, https://doi.org/10.1016/j.scriptamat.2018.08.039.
[18] S. Barbarossa, R. Orrù, S. Garroni, R. Licheri, G. Cao, Ultra high temperature high-entropy borides: effect of graphite addition on oxides removal and densification

behaviour, Ceram. Int. 47 (5) (2021) 6220–6231, https://doi.org/10.1016/j.ceramint.2020.10.200.
[19] S. Barbarossa, R. Orrù, V. Cannillo, A. Iacomini, S. Garroni, M. Murgia, G. Cao, Fabrication and characterization of quinary high entropy-ultra-high temperature diborides, Ceramics 4 (2) (2021) 108–120, https://doi.org/10.3390/ceramics4020010.
[20] S. Barbarossa, M. Murgia, R. Orrù, G. Cao, Processing conditions optimization for the synthesis and consolidation of high-entropy diborides, Eurasian Chem.-Technol. J. 23 (3) (2021) 213–220, https://doi.org/10.18321/ectj1104.
[21] G. Tallarita, R. Licheri, S. Garroni, S. Barbarossa, R. Orrù, G. Cao, High-entropy transition metal diborides by reactive and non-reactive spark plasma sintering: a comparative investigation, J. Eur. Ceram. Soc. 40 (2020) 942–952, https://doi.org/10.1016/j.jeurceramsoc.2019.10.031.
[22] L. Lutterotti, R. Ceccato, R. Dal Maschio, E. Pagani, Quantitative analysis of silicate glass in ceramic materials by the Rietveld method, Mater. Sci. Forum 87 (1998) 278–281. https://doi.org/10.4028/www.scientific.net/MSF.278-281.87.
[23] C. Musa, R. Orrù, D. Sciti, L. Silvestroni, G. Cao, Synthesis, consolidation and characterization of monolithic and SiC whiskers reinforced HfB_2 ceramics, J. Eur. Ceram. Soc. 33 (3) (2013) 603–614, https://doi.org/10.1016/j.jeurceramsoc.2012.10.004.
[24] W. Oliver, G. Pharr, An improved technique for determining hardness and elastic modulus using load and displacement sensing indentation experiments, J. Mater. Res. 7 (1992) 1564–1583, https://doi.org/10.1557/JMR.1992.1564.
[25] C.B. Ponton, R.D. Rawlings, Vickers indentation fracture toughness test. Part 1: review of literature and formulation of standardised indentation toughness equations, Mater. Sci. Technol. 5 (1989) 865–872, https://doi.org/10.1179/mst.1989.5.9.865.
[26] C.B. Ponton, R.D. Rawlings, Vickers indentation fracture tough-ness test. Part 2: application and critical evaluation of standardised indentation toughness equations, Mater. Sci. Technol. 5 (1989) 961–976, https://doi.org/10.1179/mst.1989.5.10.961.
[27] T. Wen, B. Ye, H. Liu, S. Ning, C.-Z. Wang, Y. Chu, Formation criterion for binary metal diboride solid solutions established through combinatorial methods, J. Am. Ceram. Soc. 103 (5) (2020) 3338–3348, https://doi.org/10.1111/jace.16983.
[28] S.K. Mishra, S. Das, L.C. Pathak, Defect structures in zirconium diboride powder prepared by self-propagating high-temperature synthesis, Mater. Sci. Eng. 364 (1–2) (2004) 249–255, https://doi.org/10.1016/j.msea.2003.08.021.
[29] R. Licheri, R. Orrù, C. Musa, G. Cao, Combination of SHS and SPS Techniques for fabrication of fully dense ZrB_2-ZrC-SiC composites, Mater. Lett. 62 (3) (2008) 432–435, https://doi.org/10.1016/j.matlet.2007.05.066.
[30] G. Cao, C. Estournès, J. Garay, R. Orrù, Spark Plasma Sintering: Current Status, New Developments and Challenges, 2019, pp. 1–320, https://doi.org/10.1016/C2018-0-02428-7, 978-012817744-0978-012817745-7.
[31] K.A. Kane, B.A. Pint, D. Mitchell, J.A. Haynes, Oxidation of ultrahigh temperature ceramics: kinetics, mechanisms, and applications, J. Eur. Ceram. Soc. 41 (13) (2021) 6130–6150, https://doi.org/10.1016/j.jeurceramsoc.2021.05.055.